Multiprobe Study of the Solid Electrolyte Interphase on Silicon-Based Electrodes in Full-Cell Configuration

N. Dupré, P. Moreau, E. de Vito, L. Quazuguel, M. Boniface, A. Bordes, C. Rudisch, Pascale Bayle-Guillemaud, D. Guyomard

CHEMISTRY OF MATERIALS

Article

pubs.acs.org/cm

Multiprobe Study of the Solid Electrolyte Interphase on Silicon-Based Electrodes in Full-Cell Configuration

N. Dupré,*[,†] P. Moreau,[†] E. De Vito,[‡,§] L. Quazuguel,[†] M. Boniface,[∥,#] A. Bordes,[‡,§,⊥] C. Rudisch,[†] P. Bayle-Guillemaud,[∥,#] and D. Guyomard[†]

[†]Institut des Matériaux Jean Rouxel (IMN), Université de Nantes, CNRS, 2 rue de la Houssinière, BP 32229, 44322 Nantes Cedex 3, France

[‡]LITEN, CEA, Minatec Campus, 17 rue des Martyrs, F-38054 Grenoble, France

[§]Université Grenoble Alpes, F-38000 Grenoble, France

[∥]INAC-SP2M, Université Grenoble Alpes, F-38000 Grenoble, France

[#]INAC-SP2M, CEA, F-38054 Grenoble, France

[⊥]Groupe de Physico-Chimie des Surfaces, Institut de Recherche de Chimie Paris, CNRS-Chimie ParisTech, 75005 Paris, France

Supporting Information

ABSTRACT: The failure mechanism of silicon-based electrodes has been studied only in a half-cell configuration so far. Here, a combination of ^{7}Li, ^{19}F MAS NMR, XPS, TOF-SIMS, and STEM-EELS, provides an in-depth characterization of the solid electrolyte interphase (SEI) formation on the surface of silicon and its evolution upon aging and cycling with $LiNi_{1/3}Mn_{1/3}Co_{1/3}O_2$ as the positive electrode in a full Li-ion cell configuration. This multiprobe approach indicates that the electrolyte degradation process observed in the case of full Li-ion cells exhibits many similarities to what has been observed in the case of half-cells in previous works, in particular during the early stages of the cycling. Like in the case of Si/Li half-cells, the development of the inorganic part of the SEI mostly occurs during the early stage of cycling while an incessant degradation of the organic solvents of the electrolyte occurs upon cycling. However, for extended cycling, all the lithium available for cycling is consumed because of parasitic reactions and is either trapped in an intermediate part of the SEI or in the electrolyte. This nevertheless does not prevent the further degradation of the organic electrolyte solvents, leading to the formation of lithium-free organic degradation products at the extreme surface of the SEI. At this point, without any available lithium left, the cell cannot function properly anymore. Cycled positive and negative electrodes do not show any sign of particles disconnection or clogging of their porosity by electrolyte degradation products and can still function in half-cell configuration. The failure mechanism for full Li-ion cells appears then very different from that known for half-cells and is clearly due to a lack of cyclable lithium because of parasitic reactions occurring before the accumulation of electrolyte degradation products clogs the porosity of the composite electrode or disconnects the active material particles.

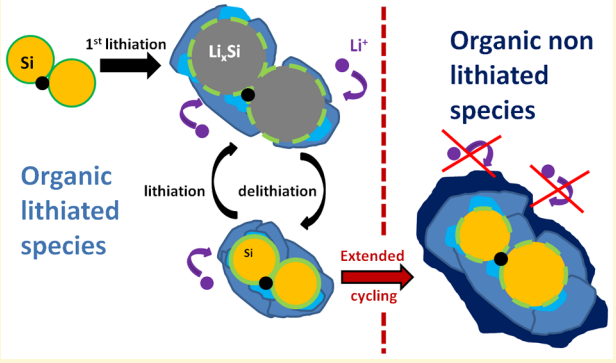

INTRODUCTION

Over the past years, lithium-ion batteries have become one of the most promising energy storage technology addressing a large range of applications, from hybrid electric vehicles, electric vehicles to plug-in hybrid electric vehicles, which are essential to reduce the fossil oil dependency. To meet requirements of these automotive applications, it is necessary to find both higher capacity and higher-capacity retention electrode materials for Li-ion batteries. Providing new materials for the negative electrode of Li-ion cells has therefore been the subject of many investigations for more than a decade. Among the candidates for negative electrode, silicon appears as an attractive alternative to graphite due to its natural abundance, high specific gravimetric capacity (3579 mAh g^{-1} vs. 372 mAh g^{-1} for graphite) and a large volumetric capacity (2081 mAh cm^{-3} vs. 779 mAh cm^{-3}). Silicon-based electrodes, however, suffer from poor cyclability because of the large volumetric expansion of Si particles upon cycling as well as to an unstable solid electrolyte interphase (SEI).[1−3] A continuous liquid electrolyte degradation occurs at the surface of the Si phase leading to the increase of the amount of electrolyte-degradation products.[4−8] The successive swelling and shrinkage upon alloying/dealloying of the stack of Si particles within the confined space of the electrochemical cell leads to major geometrical change of granular texture with a vast redistribution of interparticle contacts, the formation of cracks within the composite

Received: November 16, 2015
Revised: March 17, 2016
Published: March 17, 2016

DOI: 10.1021/acs.chemmater.5b04461
Chem. Mater. 2016, 28, 2557−2572

electrode and loss of electrical contacts at the current collector interface.[9−13] The repetition of all these processes with frictional sliding of the particles leads to a damaging of the SEI layer leading to an endless exposure of Si particles surface to the liquid electrolyte. It results in an irreversible capacity loss at each cycle by the reduction at low potential of part of the liquid electrolyte on the exposed surface.[2,6−8]

Although the interface between Si particles and the electrolyte is playing a major role in the electrochemical performance, it has rarely been characterized in depth. Moreover, all the studies attempted so far on the failure mechanism of silicon-based electrodes, were performed in a half-cell configuration where the silicon is cycled versus a lithium metal counter electrode. To our knowledge, the only study dealing with a complete Li-ion configuration[14] assigned the capacity fading of crystalline silicon/NCA batteries to a lower cycling efficiency of the cathode material at high potential, suggesting that the positive electrode material might be damaged upon cycling in addition to the electrolyte degradation. This very interesting work nevertheless does not present any fine characterization of the cell components, in particular the active materials and their SEI after cycling. From the existing literature, only the behavior of silicon electrode cycled versus lithium metal has been studied and is now well-known. Methods to optimize its performance (cyclability, lifetime, etc.) have been extensively described in the literature.[15−18] In a half-cell configuration, the supply of lithium is not limited and the failure mechanism as well as the chemical composition and properties of the SEI can be expected to be different as a significant part of electrolyte degradation products correspond usually to lithiated species. Although several reviews have already proposed SEI formation mechanisms in the case of half-cell configurations, the SEI formation scenarii were deduced from cross-linking results and data obtained from different studies, most of them focusing on one or two characterization techniques at a time.[3] In the present work, an extensive combination of techniques, ^{7}Li, ^{19}F MAS NMR, XPS, TOF-SIMS and STEM-EELS, provides both a global and in-depth characterization of the SEI forming on the surface of silicon particles as well as its evolution upon cycling in a full Li-ion cell configuration with $LiNi_{1/3}Mn_{1/3}Co_{1/3}O_2$ as the positive electrode. Such comprehensive and multitechnique characterization allows for a better understanding of the failure mechanism of Si-based composite electrodes for lithium batteries cycled in full-cell configuration since the same samples are characterized with all the techniques involved. This approach has been applied to both aged and cycled silicon samples, which are rarely studied together, and shows clearly that the chemical nature of some of the surface species is quite different in aging or in cycling mode. We show here that a proper efficient SEI is not formed by a simple exposure of the silicon surface to the electrolyte and suggests that the progressive degradation of the electrolyte upon electrochemical cycling is a completely different process compared to the calendar aging. Concerning the evolution of the SEI upon cycling, all presented experiments are original work on full Li-ion cells and were performed in such a way that they could be compared to previous studies on half cells. This allowed us to identify similarities in the SEI evolution and different failure mechanisms for half-cell and full-cell configurations, respectively. In marked contrast with typical cycling against a Li electrode, this full-cell configuration study demonstrates that the further degradation of the organic electrolyte solvents leads to the formation of SEI organic products that are lithium-free. This very important result, combined with the capacity fading and the fact that the active materials are not degraded after cycling, shows that the failure mechanism of silicon/NMC Li-ion cells is primarily due to the lack of cyclable lithium due to parasitic reactions and not to electrode degradation. Whereas in previous half cell studies failure was due to impedance rise and Si inaccessibility following SEI massive growth, we show that in a full cell, failure results from Li shortage created by an electrode slippage mechanism.

EXPERIMENTAL SECTION

Silicon Samples. The silicon power used for this study was bought from Nanostructured & Amorphous Materials (NAM). TEM analysis indicates a bimodal distribution of nanoparticle sizes, with smaller (10−40 nm) polycrystalline ones that are fused together in long chains and larger (70−150 nm) mostly monocrystalline ones (see the Supporting Information for more details).

Electrode Formulation. The negative electrode was prepared by the slurry technique, out of an aqueous dispersion. The slurry of the processed electrodes contained 8 wt % binder material (sodium-carboxymethylcellulose), 80 wt % negative active material (n-Si, 30−50 nm from nanostructured and amorphous materials) and 12 wt % conducting agent (Super P carbon black). The electrodes were not calendared. The mass loading of the negative electrodes was 0.8 mAh cm^{-2} based on a capacity limit of 1200 mAh g^{-1}. The mass loading is therefore about 1 mg/cm^2. The electrode thickness is approximately 20 μm.

The positive electrode was prepared by the slurry technique, in organic dispersion. The slurry contained 7 w% of polyvinylidenedifluoride (PVdF)-based binder, 88 wt % cathode active material (NMC) and 5 w% of the conducting agent (Super P). For the slurry preparation N-ethyl-2-pyrrolidone (NEP) was used. The slurry was coated on an aluminum current collector, adjusting the mass loads so that the specific capacity was between 0.9 and 1.1 mAh cm^{-2}. After a drying step the resulting electrodes were pressed (resulting in a reduction of the coating thickness by ∼1/3). The mass loading of the NMC (calendared) electrodes is 6.49 mg .cm^{-2} (avg. theor. cap. 0.9 mAh cm^{-2}).

Full Cell Cycling. Full batteries (Si vs NMC) were prepared in 3 electrodes Swagelok cells using $FePO_4$/$LiFePO_4$ as the reference (prepared by partial delithiation of a LFP electrode). They were cycled in 1 M $LiPF_6$ in EC:DEC carbonate electrolyte with 10w% FEC additive at limited capacity of Si electrodes (1200 mAh g^{-1}). The FEC, with a specification of below 20 ppm trace water content, was added to the electrolyte, with a specification of below 10 ppm trace water content, in the argon glovebox. Since the amount of trace water in the electrolyte containing FEC was found impossible to measure by normal KF titration, the total water content of the as prepared electrolyte is considered to be below 20 ppm. Cells were dismantled at different cycle numbers (1st, 10th, and 100th at end of lithiation and at the end of delithiation) in an argon glovebox. Table 1 gives the voltage limits for both electrodes.

Table 1. Potential Limits for the Electrodes

	silicon electrode potential (V vs Li^+/Li)	positive electrode (V vs Li^+/Li)
end of lithiation potential (limited capacity of Si: 1200 mAh g^{-1})	>5 mV	<4.2 V
end of delithiation potential	1 V	> 2.8 V

Full Cell Aging. Full cell were aged in the same configuration as for the cycling part, for different times (2 h, 1 day, 1 month) and different temperatures (at 25 and 55 °C).

Solid-State High-Resolution Nuclear Magnetic Resonance (NMR). Electrodes used for the ^{7}Li and ^{19}F MAS NMR were stopped

DOI: 10.1021/acs.chemmater.5b04461
Chem. Mater. 2016, 28, 2557−2572

at the end of delithiation or lithiation. They were then removed from the current collector inside the glovebox and placed in a cylindrical 2.5 mm diameter zircona rotor without being washed. ^{7}Li and ^{19}F MAS NMR experiments were carried out on a Bruker avance-500 spectrometer (B_0 = 11.8T, Larmor frequencies $\nu_0(^{7}\mathrm{Li})$ = 194 MHz, $\nu_0(^{19}\mathrm{F})$ = 470 MHz). MAS spectra were obtained by using a Bruker MAS probe. Spinning frequencies up to 25 kHz were used. ^{7}Li NMR spectra were acquired with a single pulse sequence and a recycle time of 30s. ^{19}F NMR spectra were acquired using a Hahn echo sequence to discard the significant contribution from the probe signal and a recycle time of 30s. All the spectra were normalized taking account the number of scans, the receiver gain and the mass of the sample. ^{7}Li and ^{19}F integrated intensities were determined by using spectral simulation, taking the spinning sidebands into account.[19]

XPS. Electrodes were stopped at the end of lithiation or delithiation. They were then removed from the cell inside the glovebox and transferred, without being washed, by using an airtight vessel to a PHIVersa-Probe II spectrometer. Electrode samples were put on an insulating double side adhesive tape, charging effects being controlled during analysis with a combination of low energy electron gun (negative charge) and low energy argon gun (positive charge). The X-ray source was an Al Kα monochromatic beam (1486.7 eV), the takeoff angle was set standard 45°. Pass energy was set to 23.5 eV for high resolution spectra acquisition, providing an energy resolution of ∼0.59 eV. Data treatment was performed within the MultiPak software. Curve fitting was achieved by using standard Shirley background subtraction and Gaussian/Lorentzian peak shapes. All spectra were calibrated by using C 1s as a reference binding energy (284.8 eV).

STEM-EELS. measurements were performed at the first, 10th, and 100th lithiation and delithiation. After cell disassembly, electrodes not rinsed and were allowed to dry at room temperature in the glovebox before TEM experiments. Washing was avoided in order not to dissolve the SEI or damage its microstructure. The dried electrodes were then gently scratched over lacey carbon films coated onto copper mesh grids. Those grids were then mounted onto a Gatan vacuum transfer holder to directly bring the sample from glovebox to microscope without any exposure to oxygen or moisture.

Battery samples were investigated using FEI Tecnai Osiris and FEI Titan SuperTwin microscopes operated at 200kV. Electron energy loss (EELS) measurements were performed in scanning transmission electron microscopy (STEM) mode, with typical experimental settings α = 4 mrad and β = 12 mrad in the Osiris and α = 0.7 mrad and β = 5 mrad in the Titan. Spectrum images (SI) were then acquired by scanning the beam across the specimen and recording EELS spectra at each position. It is well-known that electron beam damage can be quite considerable during EELS acquisition. A special method was thus developed based on low-loss measurements with decondensed probe and optimized signal-to-noise ratio. It was checked that using this method no beam damage could be evidenced and that a second mapping on the same area was giving identical results. A more detailed description of the method will be given in a forthcoming dedicated paper. In brief, since both lithium-silicon alloys and SEI species are respectively subject to knock-on damage and radiolysis under the electron beam, efforts were made to limit the dose and dose rate by (i) lowering the beam current (5pA), (ii) widening the beam to spread out the dose, either by lowering the convergence angle or defocusing, (iii) using the low-energy part of the EELS spectrum (plasmon) for which short exposure times (5−15 ms) are sufficient.

The zero-loss peak as well as second order scattering and higher orders were removed by the Fourier-log deconvolution method, and principal components analysis (PCA) was applied to the resulting spectra as a noise removal technique.[20] Chemical composition maps could then be generated by comparing experimental spectra to our reference compounds spectrum database through the multiple linear least-squares (MLLS) fitting routine.

TOF-SIMS. Electrodes were mounted on a sample holder with a double sided carbon adhesive tape. Samples were transferred directly from the glovebox to an ION-TOF ToF-SIMS preparation chamber by using a sealed transfer vessel to avoid exposure to air. Electrodes were investigated by using a 60 keV Bi_3^{+2} analysis beam and a 30 keV FIB gallium. The FIB cut was milled with a 20 nA current and then "polished" using a 5 nA current. Measurement current was 0.12 pA. Depending on the elements of interest, positive or negative secondary ions were analyzed. The vacuum during the experiments was below 5×10^{-9} mbar.

RESULTS AND DISCUSSION

1. Aging Study. The ^{7}Li NMR spectra of silicon electrodes exposed to the $LiPF_6$ (EC:DEC + 10 wt % FEC) 1 M electrolyte are compared in Figure 1a for the different aging times and temperatures. Components of the electrolyte react spontaneously at the surface of the silicon electrode as 2 resonances can be observed in the ex situ ^{7}Li MAS NMR spectra of the electrode recovered after 2 h of exposure to electrolyte at 25 °C. The sharp and well-defined resonance at 0.3 ppm can be assigned to diamagnetic lithium species such as lithiated organic carbonates or alkyl carbonates coming from the degradation of the electrolyte solvents. The broader component in ^{7}Li is also assigned to lithiated species coming from the degradation of electrolyte components and deposited on the surface of the electrode but seems to lead to a wider chemical shift distribution. This signal spans over the −1 to −3 ppm region and include the contribution of fluorinated products. PF_6^- groups are clearly identified by a sharp and well defined resonance at −72 ppm in the corresponding ^{19}F spectrum (Figure 1b). Their presence is most probably due to dried and unreacted $LiPF_6$ salt. Apart from the PF_6^- signal and a trace of unreacted FEC (−123 ppm), no other ^{19}F contribution has been detected, in particular LiF (expected at −204 ppm) suggesting that the lithiated species precipitating on the surface of the electrode are nonfluorinated and most probably organic species as it has been already observed in the literature.[21−26]

No trace of LiF, known to be one of the main SEI components have been observed by NMR.[7−10] XPS analyses indicate nevertheless the presence of small amounts of LiF at the surface of the Si electrodes aged for 2 h, at 25 and 55 °C (Figure 2a). Because XPS probes the extreme surface of the samples while NMR is primarily a bulk technique, these results suggest the presence of small amounts of LiF only localized in the outer part of the SEI. No trace of FEC or decomposition products of the FEC was detected, indicating that the FEC is well-dissolved and remains in solution. XPS results also show that Si surface remains very stable, and the native Si oxide is still very thin after aging (Figure 2b).

Limited changes were observed for a 1 day exposure time at room temperature and for 2 h at 55 °C, indicating over this short time period a good stability of both the electrolyte and the silicon/electrolyte interface. However, after 1 month at room temperature, the intensity of the ^{7}Li resonance does increase dramatically indicating a clear progress of degradation.

A significant change is also observed for 1 day and 1 month of exposure time at 55 °C (Figure 1), indicating that the degradation is thermally activated. This degradation of the electrolyte is clearly observed from both ^{7}Li NMR spectrum, with the rise of a broad and intense signal at approximately −1 ppm (1 day at 55 °C) and approximately −1.6 ppm (1 month at 25 or 55 °C). Such broad resonances are likely to contain several contributions and their slightly negative shifts suggest the presence of fluorinated compounds. In the corresponding ^{19}F NMR spectra, however, no trace of LiF at −204 ppm can be detected and only traces of unreacted FEC (−123 ppm), PF_6^- groups (−72 ppm) and a broad signal

DOI: 10.1021/acs.chemmater.5b04461
Chem. Mater. 2016, 28, 2557−2572

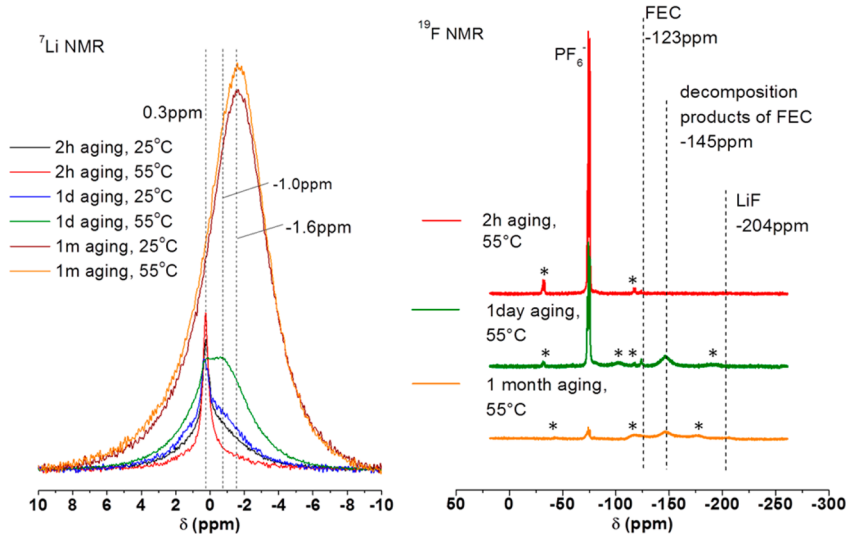

Figure 1. (Left) Normalized ^{7}Li MAS NMR spectra with all six aging conditions. (Right) Normalized ^{19}F MAS NMR for 55 °C/1 h, 55 °C /1 day, and 55 °C/1 month aging conditions. In both cases, NMR data have been normalized with respect to the mass of sample and number of scans and the spectra are given in absolute intensity. Asterisks mark the position of spinning sidebands.

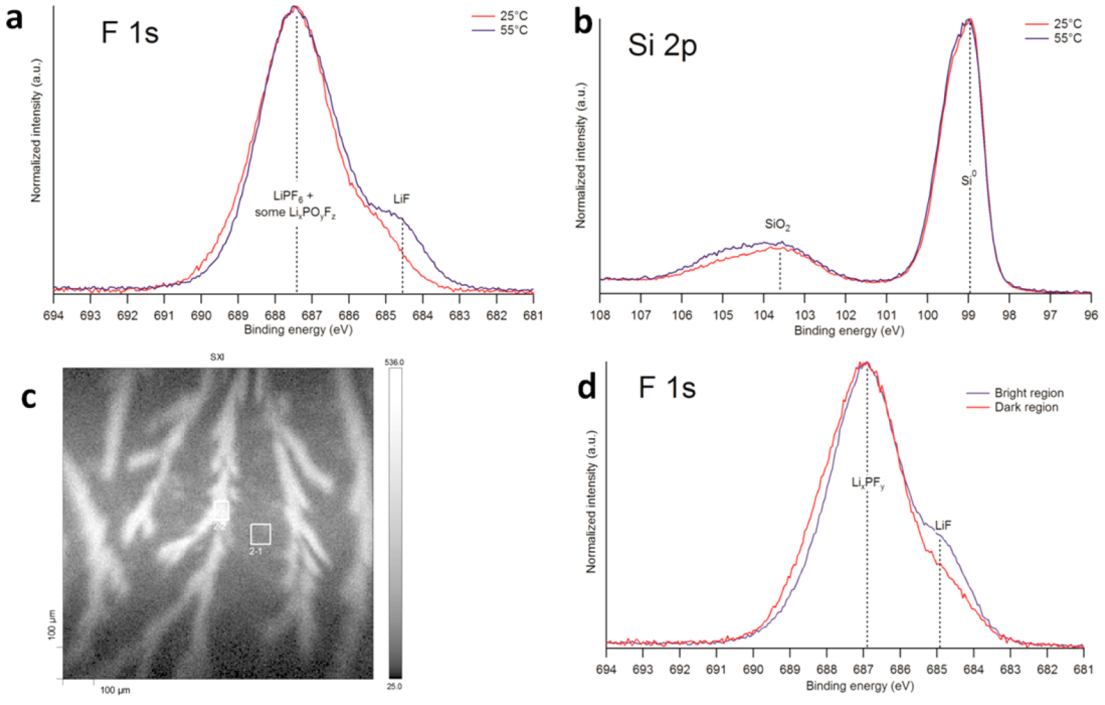

Figure 2. XPS spectra of Si electrodes aged 2 h at different temperatures: (a) F 1s and (b) Si 2p. (c) Secondary electron (SXI) image of Si electrode aged 1 day at 25 °C; (d) F 1s XPS spectra from dark and bright zones of image c.

at −145 ppm assigned to decomposition products of the FEC are observed . Since the ^{7}Li signals with apparent center at approximately −1 and −1.6 ppm seem to appear concomitantly with the broad ^{19}F resonance at −145 ppm, we tentatively assign those ^{7}Li signals to lithiated species stemming from degradation of FEC. Dried $LiPF_6$, expected in the −2 to −3 ppm range seems to be masked by the broad ^{7}Li resonances. Typical ^{19}F NMR shifts for C═C-F groups are within the −100 to −150 ppm range, which is in agreement with the observed −145 ppm chemical shift. Nevertheless, the formation of a carbon-carbon double bond is not expected from the ring opening reaction of FEC.[3] Okamoto [27] has investigated possible degradation products of FEC in $LiPF_6$ using ab initio methods. Among possible products, the most probable products obtained by the opening of the ring of FEC contain either -CHF or − CF═O. CHF group and CF═O group are expected between 20 and 40 ppm and at approximately −115 ppm, respectively. Species containing these groups can thus be ruled out. CF_2H_2 is expected at −143 ppm and species containing − CH_2F groups can be also expected in this range. Some of these species could contain lithium. At this point, a more accurate determination of the formula would require ^{13}C NMR, not developed in the scope of this work. Again, in that case, no trace of LiF is found by NMR but is still visible by XPS. Rapid degradation of the electrolyte can be expected if the functioning temperature of the cell reaches 55 °C.

DOI: 10.1021/acs.chemmater.5b04461
Chem. Mater. 2016, 28, 2557−2572

SXI images (X-ray beam induced secondary electron images) achieved on a sample aged 1 day at 25 °C shows heterogeneities at the surface. XPS analyses have been carried out on these areas. Results show that the dendrite-like zones are related to a small increase of a LiF component. The heterogeneities may be due to the deposition of $LiPF_6$, leading to a partial enrichment in LiF in these areas (Figure 2c, d).[28]

2. Cycling Study. *2.1. Cycling Behavior.* Figure 3a displays the typical specific capacity vs. cycle number obtained for a full Si/NMC Li-ion cell at a C/2 rate (1 Li in 2 h). The delivered capacity drastically decreases after only few cycles (less than 10) to reach less than 200 mAh.g^{-1} after 100 cycles. This strong capacity fading is also visible in Figure 3b displaying the galvanostatic profile

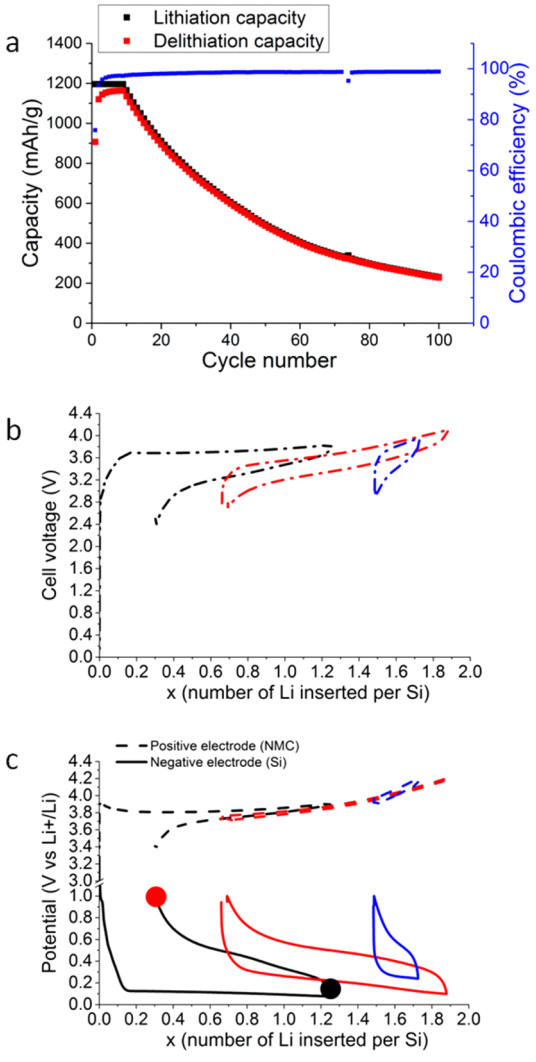

Figure 3. (a) Specific capacity curve vs cycle number for a Si/NMC cell. (b) Charge−discharge curves for a Si/NMC cell. (c) Potential of the NMC electrode (dotted line) and the silicon electrode (solid line) versus *x*, the lithium content measured in three-electrode Swagelok cells vs a $FePO_4$/$LiFePO_4$ reference and rescaled vs Li^+/Li. For clarity purpose, only the first (black), the 10th (red), and the 100th (blue) cycles are shown.

of the full Si/NMC cell. The behavior obtained for a full cell appears to be quite different from those of Si and NMC tested individually in half-cell configuration. As a matter of fact, the silicon based electrode delivers a stable capacity of 1200 mAh g^{-1} for more than 100 cycles while the NMC electrode shows a stable capacity of 120 mAh g^{-1} with no increase of the polarization, indicating very good electrochemical performance (see Figure S1).

In full-cell configuration, the positive electrode material contains the available cyclable lithium (i.e., there is no "infinite" Li ion reservoir as opposite to the case of a Li metal electrode). Figure 3c displays the galvanostatic profile of the NMC and Si electrodes for the first, 10th and 100th cycles. After 100 cycles, the potential for the silicon electrode at the end of the cell charge (lithiation of Si) is much higher (0.25 V) than for the early stage of the electrochemical cycling, indicating that its minimum cutoff potential has not been reached. On the other hand, the NMC electrode reaches its cutoff potential of 4.2V. This behavior indicates clearly that no lithium ions are available anymore from the NMC electrode to lithiate the silicon electrode. In addition, the overall high potentials of both NMC and silicon suggest that both electrodes are in delithiated or almost delithiated states after 100 cycles. The delithiated state of silicon electrode after the 100th lithiation has been confirmed by ^{7}Li NMR (see Figure S4). It is then reasonable to assume that most of the initial cyclable lithium is not within the structure of active materials but rather still in the electrolyte or contained in the SEI formed on the surface of both electrodes.

2.2. Multiscale Description of SEI Composition and Heterogeneities in Li-ion Configuration. Figure 4 (left) displays the ^{19}F MAS NMR spectra obtained for the silicon electrodes at the end of lithiation after 1, 10, and 100 cycles in Li-ion configuration. The formation of the SEI on the silicon surface is detected during the first lithiation process in agreement with previous studies.[21−26,29] At the end of the first lithiation, ^{19}F MAS NMR clearly indicates the presence of LiF at −204 ppm along with a strong signal assigned to PF_6^- groups (doublet at −72 and −74 ppm) and corresponding either to dried unreacted electrolyte or $LiPF_6$ trapped in the porosity of the SEI. The slightly different apparent shift observed for the PF_6^- groups, in the case of the 10th lithiation suggests a higher contribution of dried $LiPF_6$ with respect to confined liquid $LiPF_6$. In the ^{7}Li MAS NMR spectrum obtained at the end of the first lithiation (Figure 5), two sets of resonances are observed. The first one, centered at 1.6 ppm has been assigned to Li_xSi alloys, whereas the second centered at −0.5 ppm can be assigned to diamagnetic lithiated surface species. Although the apparent shift is measured at −0.5 ppm, the signal is quite broad, exhibiting a chemical shift distribution due to the variety of Li chemical environments, including LiF typically along with lithiated alkyl carbonates.[7,30,31] As a matter of fact, the signal seems to mask the expected LiF signal at −1 ppm. It suggests that only a minor part of the detected lithiated diamagnetic species corresponds to LiF. This broad resonance centered at −0.5 ppm is also observed at the end of the first delithiation (Figure 4, right) where only Li in the SEI is expected.

In the present case, the chemical shift observed for the lithiated alloys Li_xSi_y at 1.6 ppm (Figure 5) is quite different from data that can be found in the literature where lithium poor alloys rise at 18 ppm and lithium rich alloys at approximately 6 ppm.[7,32] Those shifts are observed in the case of the lithiation mechanism starting from crystallized silicon. In the present study, the silicon used is nanostructured and a slightly different lithiation mechanism could lead to the detection of different Li_xSi signals.[33] Although the silicon electrode recovered at the end of lithiation correspond to a partial lithiation of 1200 mAh g^{-1},

DOI: 10.1021/acs.chemmater.5b04461
Chem. Mater. 2016, 28, 2557−2572

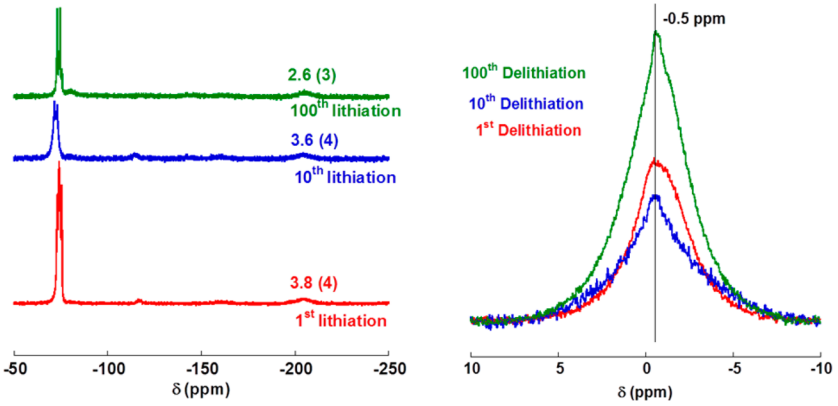

Figure 4. (left) Normalized ^{19}F MAS NMR spectra of silicon electrodes, at the end of 1st, 10th, and 100th lithiation in Li-ion configuration. The integrated intensity (arbitrary unit) values for LiF are given above the corresponding resonance at −204 ppm. (right) Normalized ^{7}Li MAS NMR spectra obtained at the end of 1st, 10th, and 100th delithiation. NMR data have been normalized with respect to the mass of sample and number of scans and the spectra are given in absolute intensity.

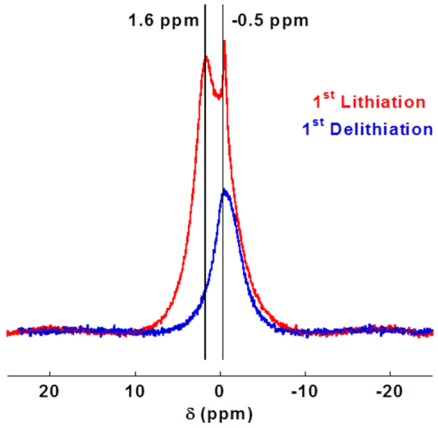

Figure 5. Normalized ^{7}Li MAS NMR spectra of silicon electrodes, at the end of first lithiation and first delithiation in Li-ion configuration. NMR data have been normalized with respect to the mass of sample and number of scans and the spectra are given in absolute intensity.

lithium poor alloys are clearly not detected. The signal centered at 1.6 ppm and assigned to Li_xSi alloys is quite broad and could overlap with resonances between 0 and 6 ppm. Such signal could therefore contain a distribution of Li local environments and several Li_xSi_y compositions. As a matter of fact, similar behavior has been observed for silicon nanowires consisting in a crystalline core with an amorphous shell.[34] In this case, it becomes quite difficult to distinguish surface Li (in the SEI) and Li in the Li_xSi alloys due to strongly overlapping lines. The resonance obtained at the end of the first delithiation can be nevertheless fitted by a single broad Gaussian peak, suggesting that there is no contribution of an additional resonance at 1.6 ppm although it is not possible to rule out the presence of a minor contribution of Li_xSi. In that case, such a contribution would be masked by the SEI contribution and would be negligible.

In a first approximation, the NMR integrated intensity ratio between lithiated state (containing Li within the alloy and in the SEI) and delithiated state (containing Li in the SEI only) can be compared to the ratio from electrochemistry between the total capacity (Li within the alloy and Li involved in the SEI formation) for the first lithiation and the irreversible capacity at the end of the first delithiation (remaining Li in the SEI). Values of 0.50 and 0.24 are found for NMR data and electrochemical data, respectively. Although there is a clear discrepancy, this result confirms the presence of Li within the silicon alloy at the end of lithiation and its extraction at the end of delithiation. The discrepancy could be explained by the existence of parasitic reactions between electrolyte components and the active material, involving electrons but no lithium, as discussed later on in part 2.4.

Complementary to the NMR results on the SEI formation, XPS F1s spectrum in Figure 6 (top) confirms the presence of LiF, in addition to other lithiated species such as Li_xPF_y or $Li_xPO_yF_z$. The contribution of broad peaks in the C1s spectrum in Figure 6 (bottom) suggests that the degradation of organic solvents, involved in the SEI formation, has also already started. C 1s contributions in Figure 6 (bottom) are typically observed on SEI formed after carbonate-based electrolyte degradation on Si after 1 to a large number of cycles.[35,36] There seems to be no significant difference in the chemical nature of species coming from the degradation of the solvents during the early stage of cycling in the case of half-cell and Li-ion cell.

XPS analyses also allow the observation of Si chemical states. After the first lithiation, 3 main contributions can be observed at increasing energy shifts in Figure 7, corresponding to Li_xSi, Si°, and Li_xSiO_y compounds, respectively.[20,28] Li silicates are known to form after the first cycle and to contribute to the irreversibility of the first cycle. In our case, after 10 cycles, the situation did not evolve much for Si. After 100 cycles, only the Li_xSiO_y contribution can be observed. These results show that, during cycling (i) Li_xSiO_y is formed in high quantities and (ii) Si° signal progressively disappears as SEI is becoming thicker. Less and less Si can be accessed and is thus available for cycling. The formation of Li_xSiO_y in significant amount is a clear indication that the surface of the silicon is involved in the reaction with the electrolyte and probably participates in reversible capacity fading. Such a reaction necessarily involves an exchange of electrons between the native silicon surface and components of the electrolyte as the silicon oxidation state changes (from 0 to + 4 in the case of the formation of Li_4SiO_4).

Although NMR and XPS give average results and lack of spatial resolution, STEM-EELS is a perfectly appropriate tool to probe the inhomogeneities in the chemical composition of the SEI and describe the distribution of species coming from the degradation of the electrolyte on the surface of silicon particles. In addition, STEM-EELS allows probing the SEI in the core of the electrode and not only the surface. STEM-EELS analyses

DOI: 10.1021/acs.chemmater.5b04461
Chem. Mater. 2016, 28, 2557−2572

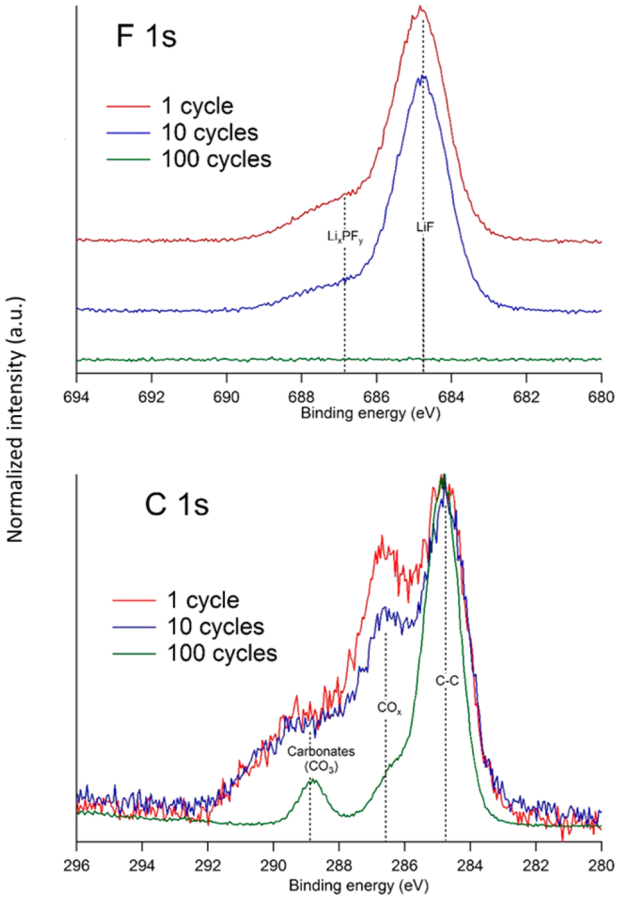

Figure 6. (top) F 1s and (bottom) C 1s XPS spectra of Si electrodes after 1st, 10th, and 100th (end of lithiation) in Li-ion configuration.

performed at the end of the first lithiation clearly detect thick patches of LiF, even on unlithiated nanoparticles, and carbonates on the surface of silicon particles or sandwiched between two or more silicon particles (Figure 8a, b). These results indicate that from the early stage of the electrochemical cycling, the SEI does not appear as an uniformly covering layer at the surface of silicon grains but rather as inhomogeneous deposits. These deposits are present not only at the surface of Si grains that have been lithiated but also on grains that have not yet been involved in the redox process. Therefore, from a topological point of view, STEM-EELS results emphasize the fact that the SEI does not appear as a continuous and homogeneous layer neither on the electrode scale nor at the nanoparticle scale. These extremely local analyses cannot however probe the full depth of the electrodes. It has been shown that on thick electrodes, the SEI can be distributed unevenly from the electrolyte-electrode interface to the current collector-electrode interface. Depth profiling across the entire electrode was thus performed through ToF-SiMS thanks to in situ FIB cuts (Figure 9).

In the secondary electron image of the whole FIB crater (Figure 9a) the surface of the electrode is visible and cracks can be identified. These cracks can be the result of successive expansion and contraction of the electrode and they extend right through the whole electrode thickness down to the current collector.[37]

This method allows carrying out chemical mapping on the cross-section, giving good qualitative results, which reveal inhomogeneities at a much larger scale than STEM-EELS. For quantitative analysis, other techniques like XPS are more appropriate for this kind of samples. Figure 10 presents Li^+, P^+, and F^- distributions across the electrode after the first lithiation. At this stage, a slight inhomogeneity in the distribution of lithium, fluorine, and phosphorus is already worth noting. These inhomogeneities could be the result of a poor distribution of the SEI in the depth of the electrode. In particular, close to the current collector, large patches containing Li, P, and F can be identified. This accumulation may contribute to the progressive delamination of the electrode. Elemental maps of Li^+, Si^+, and P^+ after the first delithiation are shown in Figure 11. Lithium distribution indicates a homogeneous delithiation of the electrode. The detection of lithium is attributed to lithium trapped in the SEI, leading to the first irreversible capacity loss. On the contrary, silicon maps exhibits inhomogeneities with higher intensity areas attributed to an uneven SEI coverage.

From the multiprobe and multiscale observation of the SEI forming at the silicon electrode at the beginning of the electrochemical cycling, it appears that its composition and topology display the same overall properties as those observed in the case of silicon half-cells. Both the nature of chemical

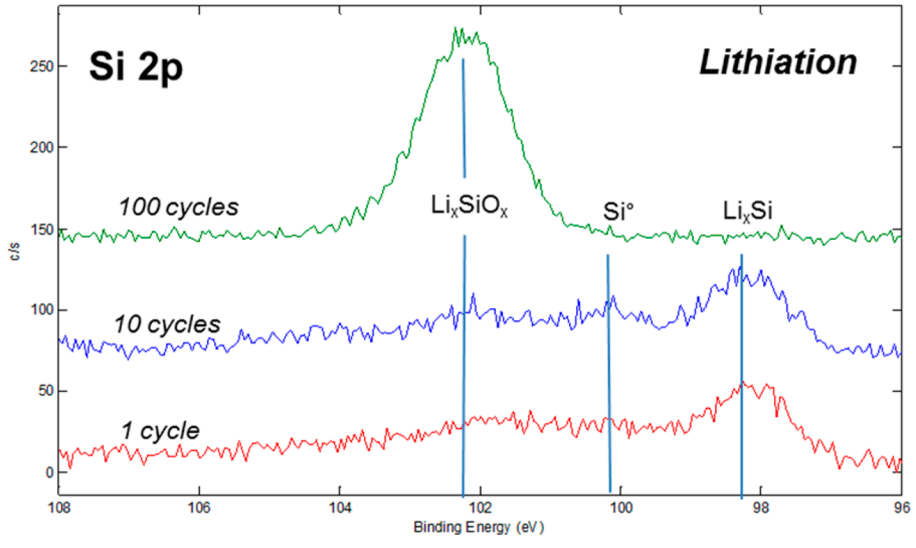

Figure 7. Si 2p XPS spectrum of silicon electrodes at the end of lithiation for 1, 10, and 100 cycles in Li-ion configuration.

DOI: 10.1021/acs.chemmater.5b04461
Chem. Mater. 2016, 28, 2557−2572

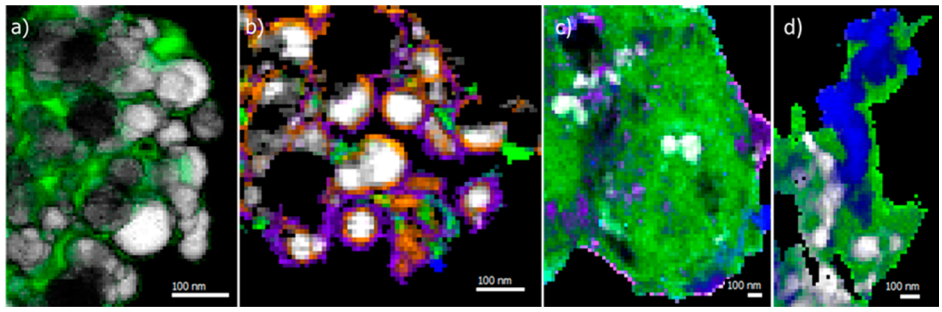

Figure 8. Mapping of silicon (gray to white), Li_xSi alloys (orange), LiF (green), carbonates (purple), and carbon black (blue), calculated from STEM-EELS measurements. The scale bar is 100 nm. (a) Unreacted Si surrounded by thick patches of LiF after the 1st lithiation. (b) Core−shell structure of lithiated silicon surrounded by LiF patches and a ∼ 20 nm thick carbonate layer after the 1st lithiation. Large SEI build-ups after the (c) 100th lithiation and (d) 100th delithiation.

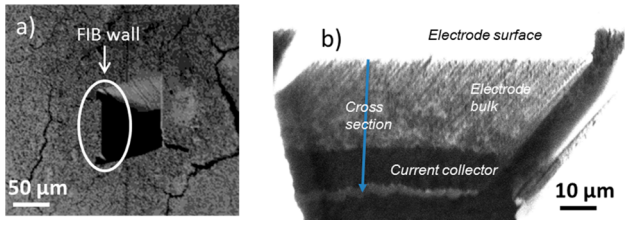

Figure 9. In situ FIB cut of a silicon electrode performed after the first delithiation in Li-ion configuration, secondary electron imaging of: (a) Top view of the FIB cut and electrode surface. (b) Entire depth of the electrode.

species detected, coming from the degradation of electrolyte salt (LiF and fluorophosphates) and solvents (organic carbonates and alkyl carbonates) and their heterogeneous distribution at the scale of silicon particles/aggregates and at the scale of the electrode cannot explain directly the (faster) failure mechanism in the case of the Si/NMC Li-ion cell. The particular and unique evolution of such SEI in the complete Li-ion configuration is now investigated.

2.3. Particularities of SEI in Li-Ion Configuration. To determine the possible existence of a correlation between the SEI, as described in the previous section, and the electrochemical performance, its evolution in terms of chemical composition has been monitored over 100 cycles and is described in the present section.

In Figure 12 (left) the evolution of Li, C, and O content in the SEI, deduced from XPS measurements displayed in Figure 6, is plotted as a function of the cycle number (end of lithiation). For each element, the specific contributions closely related to the SEI were considered, in particular: (1) for F 1s, Li-F bonds, (2) for C 1s, CO_x/C−C bonds (excluding C−C bonds from the graphite-based conductive additive), (3) for Li 1s and O 1s, Li and O contributions excluding the respective lower binding energy peaks related to Li or Si oxides. Fluorine, lithium, and oxygen contents are quite stable up to 10 cycles, then a high decrease of their relative content is observed. At the same time, carbon content greatly increases up to 80 at % when reaching 100 cycles. Two effects can be considered:

(1) Up to 10 cycles, there is an enrichment of the SEI in LiF, explaining the high Li and F content in the SEI together with carbonates degradation leading to $ROCO_2Li$ compounds. The latter compounds are related to the CO_x peaks shown in Figure 6 (bottom).

From 10 to 100 cycles, there is a high enrichment in carbon-based compounds at the expense of lithium and fluorine-based species, which are surprisingly not detected at all at the electrode surface. Moreover, as underlined in Figure 12, carbon compounds must not be related to $ROCO_2Li$ species, because lithiated species are not detected. Indeed, even for a long acquisition time no intensity could be detected on the Li 1s XPS spectrum (Figure 12, right), after 100 cycles. It confirms clearly that all the cyclable Li has been entirely consumed in parasitic reactions before the 100th electrochemical cycle has been reached. It indicates also that species present at the extreme surface of the SEI, within the 5 nm penetration depth of the XPS beam, are nonlithiated. The absence of detectable fluorine confirms the absence of LiF at the extreme surface of the SEI. It suggests also that the unreacted $LiPF_6$ detected by NMR is likely to be trapped in the porosity of the SEI and not simply at the surface of the electrode.

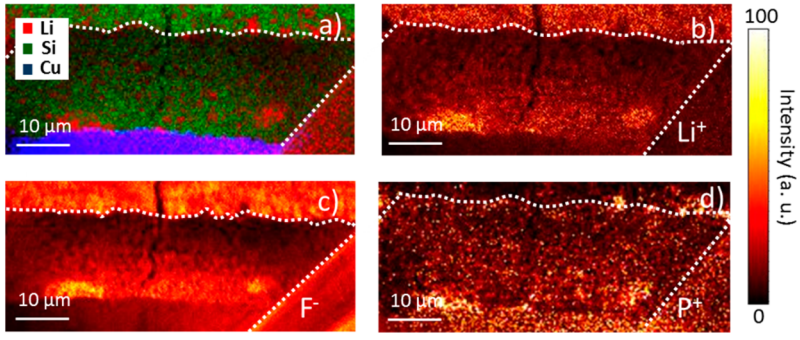

Figure 10. ToF-SIMS chemical imaging of a silicon electrode FIB cross section obtained by in situ FIB cut performed after the first lithiation in Li-ion configuration, a) Overlay of Li^+, Si^+, Cu^+ maps. (b) Li^+ maps. (c) F^- maps. (d) P^+ maps. Dashed white lines delimitate the cross-section wall.

DOI: 10.1021/acs.chemmater.5b04461
Chem. Mater. 2016, 28, 2557−2572

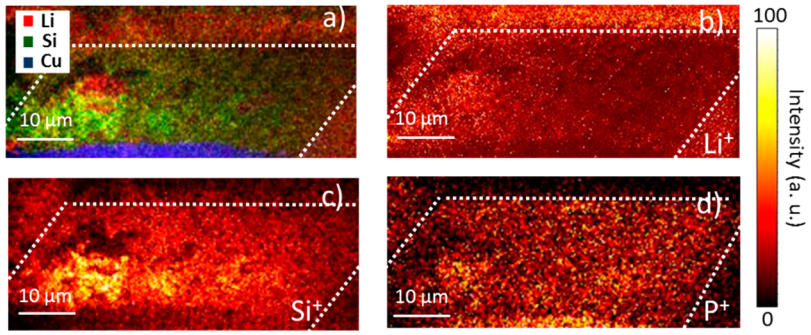

Figure 11. ToF-SIMS chemical imaging of a silicon electrode FIB cross-section obtained by in situ FIB cut performed after the first delithiation in Li-ion configuration. (a) Overlay of Li^+, Si^+, Cu^+ mappings. (b) Li^+ mapping. (c) Si^+ mapping. (d) P^+ mapping. Dashed white lines have been added to delimitate the cross-section wall. Cross-comparison of the elemental maps reveals a fairly homogeneous distribution of Li in opposition with the high intensity areas in Si signal.

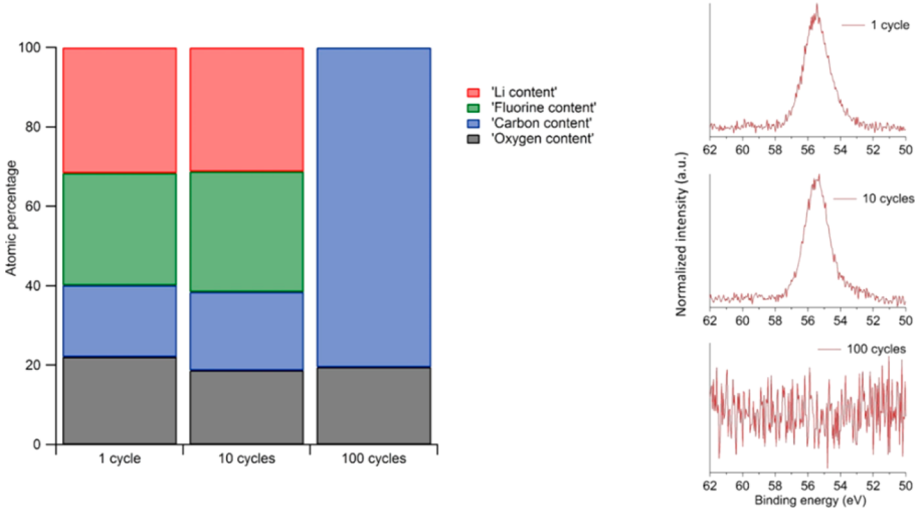

Figure 12. (Left) Evolution of Li (red), C (blue), O (black), and F (green) content in the SEI at the silicon electrode surface at the end of lithiation in Li-ion configuration, as a function of the cycle number, deduced from XPS measurements. (Right) Li 1s XPS spectra of silicon electrodes after 1, 10, and 100 cycles in Li-ion configuration.

The high enrichment in carbon-based compounds explains the relative decrease of CO_x contribution in favor of CO_3 and C-C contributions after 100 cycles. The formation of polymeric species with significant CO_3 and C-C contributions has been already proposed in previous studies.[23,26,38,39]

(2) It is well-known that part of the electrolyte decomposition products are gaseous.[40] From the theoretical point of view, Okamoto has investigated possible degradation products of EC and FEC in $LiPF_6$ using ab initio methods. Among possible products obtained by the opening of the ring of FEC, the release of CO_2 is also predicted.[27] It has also been shown in previous works that the degradation of the electrolyte not only leads to the formation of the SEI, but also to the release of soluble oligomers containing oxygen atoms[41] such as $C_9H_{18}O_5$, $C_{13}H_{26}O_7$, or $C_{15}H_{32}O_6$. This generally occurs through degradation mechanisms inducing the formation of radicals.[39] This can explain the relative oxygen depletion observed compared to carbon, which is probably due to carbonate degradation leading to oxygen-rich compounds, soluble in the electrolyte or gas.

The evolution of the amount of LiF has been monitored over the course of the electrochemical cycling, from first to 100th cycles, using ^{19}F MAS NMR, probing the whole thickness of the SEI deposits. As it can be seen from the values of integrated intensity of the LiF peak (Figure 4, left), no clear accumulation of LiF can be detected. A similar result is obtained concerning the set of resonances between −72 and −75 ppm, assigned to dried or trapped $LiPF_6$ and possibly fluorophosphates.[42] It clearly indicates that fluorinated species constituting the inorganic part of the SEI tend to form during the early stage of the cycling, mostly during the first lithiation and seem to be quite stable upon cycling. Contrary to ^{19}F NMR results, the integrated intensity of the ^7Li signals recorded for samples at the end of delithiation (containing only or mostly lithium involved in SEI) clearly increases (Figure 4, right) between the early stage of cycling (1 and 10 cycles) and the end of the electrochemical cycling (100 cycles). It confirms the accumulation of lithiated and nonfluorinated species in the SEI over the course of 100 cycles. These additional lithiated species can be attributed either to inorganic Li_2CO_3 or lithiated organic species such as alkyl carbonates, known to form from the degradation of electrolyte solvents.[3,26] The formation of Li_2CO_3 can be nevertheless ruled out as it usually forms if moisture is present during sample preparation,[43] which is unlikely because the samples were kept in an argon glovebox (H_2O content < 0.1 ppm) and transferred to the analysis equipment using airtight sample holders.

DOI: 10.1021/acs.chemmater.5b04461
Chem. Mater. 2016, 28, 2557−2572

The evolution of the SEI described from the NMR data is in agreement with the stable contribution of LiF deduced from XPS analyses (Table 2) for all the samples investigated except the silicon electrode at the end of delithiation after 100 cycles. In that particular case, the contribution of carbonaceous species containing C-O, CO_2 and CO_3 groups shows a clear increase. After 100 cycles, as discussed above, carbonates formed at the outermost surface are non lithiated. Considering the limited amount of lithium available in full-cell configuration, it is reasonable to assess that the degradation of the electrolyte solvents still occurs when most of the lithium is already trapped in the SEI, leading to lithium poor and lithium free polymers at the extreme surface of the SEI. This phenomenon is a clear difference from observations in half cell configuration where Li is in unlimited supply. Since the XPS technique typically probes the outer surface (5 nm), it indicates that the LiF and other lithiated species could be covered by carbonates from the solvents or organic species produced by their degradation, therefore screening the contribution of lithiated species formed during the early stages of the electrochemical cycling.

Table 2. Evolution of Relative Concentrations of Specific Contributions, from the SEI and from the Active Material, As a Function of Cycle Number (produced from XPS data)

comp (at %)[a]	C	Li-F	F-Li	O	P	Si
1 lith.*	17.3	30.4	27.3	21.3	2.5	1.2
1 delith.*	37.1	17.1	17.6	23.9	2.3	2
10 lith.	19.1	30.2	29.4	18.1	1.9	1.3
10 delith.	19	32	30.3	15.5	2	1.2
100 lith.	78	0	0	18.9	0	3.1 (Li_xSiO_x)
100 delith.	75.6	0	0	18.5	0	5.9 (Li_xSiO_x)

[a]"x (de)lith." means "after x electrochemical cycle, at the end of (de)lithiation"

Such a trend in the "stacking" or distribution of the different species found in the SEI is also depicted in STEM-EELS images displaying the presence of the thick patches of LiF already mentioned partially covered by a layer of organic products including carbonates (Figure 8). Such trend has been previously observed for positive electrode materials as well.[44,45] The accumulation of SEI is also visible in the STEM-EELS maps (figure 8 c and d) exhibiting very large amounts of SEI present on the surface of silicon particles. This layer reaches a thickness of tens of nanometers, considerably larger than the sampling depth achieved by XPS lab equipment, confirming that the XPS contributions from species in the inner part of the SEI could be completely masked by contributions from organic species in the outer part of the SEI deposits.

Other TOF-SIMS measurements were performed at (de)-lithiated states after 100 cycles and are presented in Figure 13. In both states, the overlay of silicon and lithium maps reveals that the pronounced inhomogeneity in the lithium distribution is still present, showing an irregular SEI repartition. The uneven Li distribution affects in particular the deeper region of the electrode. Regarding Figure 13b and the cell bad performance at this point of cell lifespan, a poor delithiation of the electrode can be suspected. Nonetheless considering NMR results, Li is more likely trapped in SEI than in silicon. Such a heterogeneous distribution of SEI patches seems to leave some of the silicon surface bare or only covered with a thin layer of SEI, strengthening the interpretation of the detection of silicon or silicon oxide by XPS at the surface of some of the samples (see part 2.2).

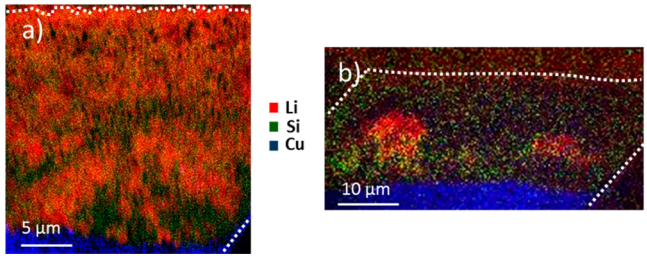

Figure 13. Overlay of ToF-SIMS chemical imaging of Li^+, Si^+, Cu^+ of the in situ FIB cut performed after 100 cycles in Li-ion configuration. (a) Lithiated state. (b) Delithiated state. Dashed white lines have been aded to delimitate the cross-section. The analysis of elemental maps reveals pronounced inhomogeneity in lithium distribution after 100 cycles.

From these results, although the inhomogeneity of the SEI in terms of chemical composition is kept throughout the electrochemical cycling, a clear trend can be pointed out in the case of full Li-ion cell configuration. The species resulting from the degradation of the electrolyte organic solvents are lithiated during the early stages of cycling but after an extended cycling, only nonlithiated species precipitate and form the external part of the SEI. This process specially occurs when the cyclable lithium supply has ceased and further degradation of solvents still proceeds. The absence of lithiated species in the external part of the SEI thus appears as a clear sign that all the cyclable lithium has been consumed. This result is supported by the comparison of ^{7}Li MAS NMR spectra of silicon electrode obtained after 100 cycles, for both a Si/NMC Li-ion cell and a Si/Li half cell cycled in similar conditions (Figure 14).

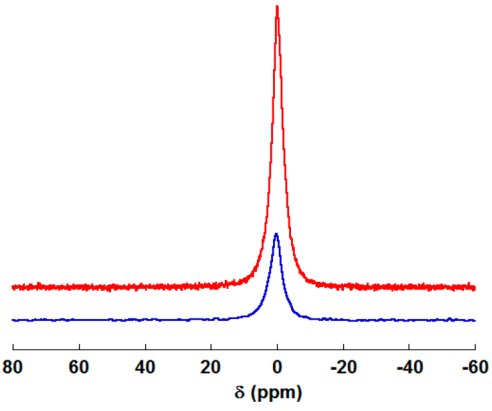

Figure 14. Normalized ^{7}Li MAS NMR spectra of silicon electrodes, at the end of the 100th delithiation for a Si/Li half cell (red) and Si/NMC Li-ion cell. NMR data have been normalized with respect to the mass of sample and number of scans and the spectra are given in absolute intensity.

From the integrated intensities ratio, the amount of lithium ions trapped in the SEI in the case of the Si/NMC Li-ion cell is approximately three times lower than that in the case of the Si/Li half-cell.

This difference is assigned to the formation of a higher amount of electrolyte degradation lithiated species due to the "unlimited" supply of cyclable lithium from the lithium metal electrode. It suggests that lithiated species will form through parasitic reactions as long as lithium ions are provided from the electrodes. This process becomes limited in the case of the Si/NMC Li-ion cell. This result can be pointed out as very important as this process can have a strong impact on the

DOI: 10.1021/acs.chemmater.5b04461
Chem. Mater. 2016, 28, 2557−2572

failure mechanism of lithium batteries depending on which phenomenon is occurring first: degradation of the active materials, clogging of the electrode porosity by thick SEI deposits or consumption of cyclable lithium in parasitic reaction.

2.4. Dynamic Nature of the SEI and Parasitic Reactions Leading to Slippage Process. To further investigate the correlation between parasitic reactions and lithium consumption, the evolution of the SEI can be also followed more specifically in its dynamic aspect, by comparing measurements corresponding to the end of lithiation and the end of delithiation for the same cycle number. After the first cycle (end of delithiation), the percentage of organic degradation products, deduced from XPS analyses, increases, whereas the contribution of LiF decreases compared to the previous end of lithiation (Table 2). After 10 cycles, this variation stabilizes and there is no significant variation of the ratio between lithiation and delithiation. These variations are consistent with the (at least) partial covering of LiF by organic species discussed above and moreover suggest (i) a dynamic behavior of the organic part of the interphase and (ii) the formation of some of the organic species during the delithiation step, in agreement with previous studies on Si/Li half cells.[3] A possible partial dissolution of LiF upon oxidation could also explain these variations. This would also explain the fluctuations of the ^{7}Li NMR integrated intensity observed after 1, 10, and 100 delithiations (Figure 4, right).

The intensity of the ^{19}F MAS NMR normalized spectra assigned to LiF (Figure 15) is besides lower when the sample is recovered at the end of delithiation than at the end of lithiation, confirming the lower amount of LiF in the SEI after the oxidation process. Between the end of the first lithiation and the end of the first delithiation, the relative amount of LiF is divided approximately by a factor of 2. Considering a typical 10% error (determined experimentally, attributed to the fit of the NMR data and the sample mass error), this variation is significative. Thus, the variation of the LiF amount deduced from XPS measurement cannot be explained only by the covering of LiF deposits by organic products, screening its XPS signal. It indicates that the amount of LiF within the SEI is clearly subject to potential variation. A similar variation, although to a lesser extent, is also seen between the end of the 10th lithiation and the end of the 10th delithiation, supporting results found for the first cycle.

Although there seems to be a trend concerning the distribution of chemical species in the SEI depth, with LiF being deeper and covered by organic species, STEM-EELS experiments show that the SEI is not homogeneous in term of chemical composition and some LiF can exist at or near the surface of the SEI. Such LiF particles or clusters exposed to the electrolyte might be subject to redissolution upon potential increase during the oxidation process. Such variations of the LiF quantity have been also detected for other negative electrode materials.[46,47] After the 100th lithiation, spectrum imaging by STEM-EELS shows that silicon particles appear to be trapped inside a thick LiF matrix covered by a carbonate layer. After the subsequent delithiation (i.e., the 100th delithiation), this carbonate layer could not be observed anymore (Figure 8c, d), confirming previous results and suggesting that the dynamic nature of the carbonate part of the SEI is still observed even after the failure of the cell.

Such a dynamic nature of part of the SEI is typically assigned to parasitic reactions involving components of the electrolyte.

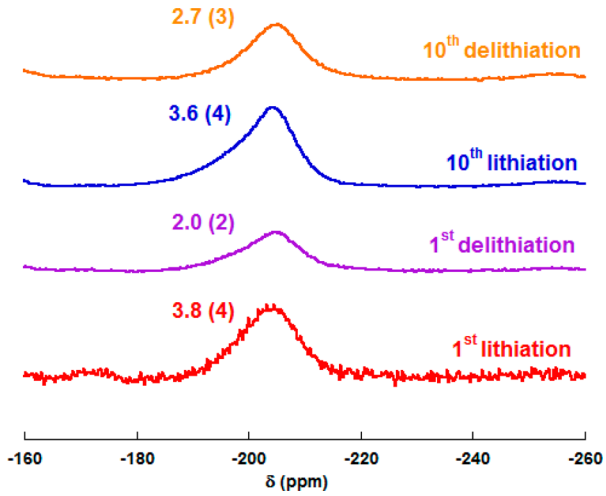

Figure 15. Normalized ^{19}F MAS NMR spectra of silicon electrodes obtained at 1st and 10th cycles at the end of lithiation and delithiation, in Li-ion configuration. The integrated intensity (arbitrary units) values for LiF are given above the corresponding resonance at −204 ppm.

These parasitic reactions are also suggested by the comparison of the amount of Li nuclei counted by ^{7}Li NMR with the amount of electrons counted by coulometry and extracted from the electrochemical data (Figure 16). The difference in chemical shift for the apparent resonances at 2.1 and 0.5 ppm with respect to the values found at the end of the first lithiation (1.6 and −0.5 ppm, respectively) can be assigned to slightly different Li_xSi compositions and different contributions of lithiated species in the SEI(such as lithiated organic species and LiF), respectively. For a theoretical functioning of the cell, without parasitic reactions, 1 electron counted by coulometry corresponds to 1 lithium ion reacting with silicon or extracted from the alloy. In that case, the value of the composition at the end of discharge and the value of the irreversible capacity, corresponding to the lithium trapped in the composite electrode should be proportional to the amount of Li nuclei detected by ^{7}Li NMR at the end of discharge and charge, respectively. Although NMR is not an absolute quantitative method, the integrated intensity is directly proportional to the amount of detected lithium, therefore, it can be quite informative to compare ratios of NMR integrated intensities with ratios of specific capacities. In the case of the first cycle, a clear discrepancy is found between the ratio of cumulative irreversible capacity vs. total capacity (0.24) on one hand and ^{7}Li integrated intensity at the end of delithiation vs. ^{7}Li integrated intensity at the end of lithiation (0.5) on the other hand. A similar result is found for the 10th cycle, when the cell is still delivering a significant reversible capacity, the ratio of cumulative irreversible capacity (marked by a red arrow in Figure 16 (left) vs. total capacity (marked by a black arrow on Figure 16 (left) is found to be 0.30, whereas the ratio of ^{7}Li integrated intensity at the end of delithiation vs. ^{7}Li integrated intensity at the end of lithiation equals 0.40 (Figure 16, right). These discrepancies indicate that an exchange of electrons not linked to an exchange of Li^+ ions is recorded and can occur. It confirms the existence of parasitic reactions not involving lithium ions, either on oxidation or on reduction in the case of a Si/NMC full Li-ion cell configuration. Such parasitic reactions have been also detected in previous study concerning silicon based electrodes cycled in half-cell configuration[24] and full-cell $LiFePO_4/Li_4Ti_5O_{12}$ configuration[47] and lead to the formation

DOI: 10.1021/acs.chemmater.5b04461
Chem. Mater. 2016, 28, 2557−2572

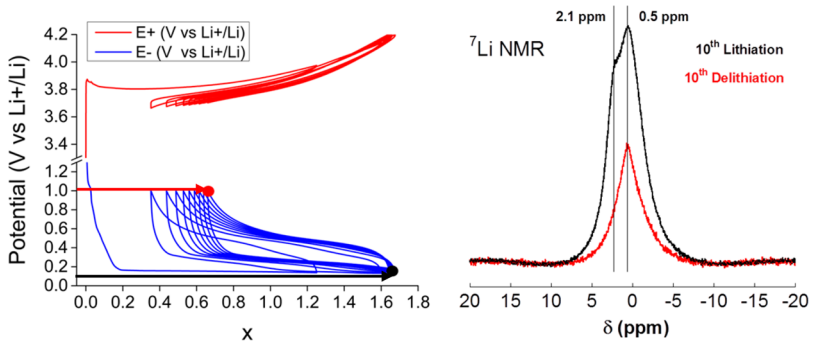

Figure 16. (left) Cycling curves of a Si/NMC full cell up to the 10th cycle. The black dot corresponds to the 10th lithiation and the red dot corresponds to the 10th delithiation, (right) corresponding normalized ^{7}Li MAS NMR spectra. NMR data have been normalized with respect to the mass of sample and number of scans and the spectra are given in absolute intensity.

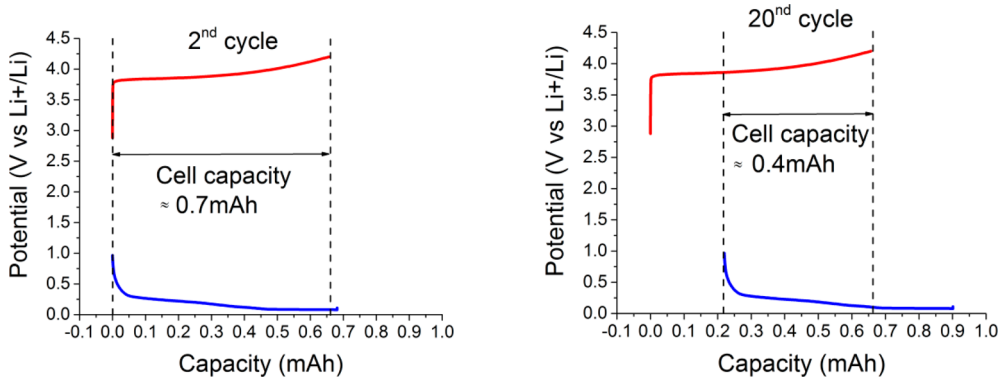

Figure 17. Voltage/capacity curves for the NMC and silicon electrode for the 2nd cycle (left) and 20th cycle (right).

of large organic molecules which are not necessary lithiated or can be poorly lithiated. This result suggests a competition between the formation of lithiated degradation products and nonlithiated degradation products. The former seems to form preferentially during the early stage of the cycling, due to the existing lithium supply, whereas the latter becomes dominant when all the cyclable lithium has been consumed.

A close examination of the voltage profiles curves for the NMC and for the silicon electrodes upon cycling indicates clearly that the parasitic reactions of electrolyte degradation leads to a stronger consumption of cyclable lithium at the negative electrode side, causing a stronger "slippage" of the corresponding voltage/capacity curve with respect to the positive electrode voltage/capacity curve and narrowing the functioning capacity window. The positive electrode thus shows a progressive decrease in its lithiation capability. This process is schematized in Figure 17.

At this stage, it becomes important to determine whether the parasitic reactions are simply consuming cyclable lithium or also leading to the clogging of electrode porosity/disconnection of active material particles by the formation of thick SEI deposits. NMC and silicon electrodes were retrieved after 100 cycles (in full Li-ion cell configuration). The electrodes were not rinsed to prevent the alteration of the existing SEI. Each electrode was then cycled in half-cell configuration with a fresh Li metal electrode and fresh electrolyte.

Figure 18 displays the corresponding specific capacity vs cycle number for both NMC and silicon electrodes. Both can still deliver excellent electrochemical performance over 60 cycles and were obviously not degraded by their cycling in full Li-ion cell configuration. This result allows confirming that the NMC and silicon active materials were not significantly degraded or altered and that the electronic and ionic percolating networks are still effective. The porosities of the electrodes, in particular that of the silicon, are thus not blocked by a thick SEI, contrary to the case of silicon electrodes cycled with similar conditions (i.e., with a limited 1200 mAh g^{-1} capacity) in half-cell configuration. From STEM-EELS results (Figure 8), the formation of large and thick patches of SEI between silicon particles is observed This process is however not significant enough to clog the porosity, the lack of cyclable lithium occurring first. The failure mechanism of Si/NMC Li-ion cell can then be described mainly by the existence of parasitic reactions leading to a lack of cyclable lithium in the full cell, long before the degradation of the electrodes or electrode materials. This process is clearly detected by the presence of only nonlithiated degradation product in the external part of the SEI.

2.5. SEI Evolution Scenario. Aging Study. NMR and XPS analyses of samples aged at different temperatures (25 and 55 °C) and for different durations (2 h, 1 day, and 1 month) in full Li-ion cell configuration indicate, in agreement with previous studies on half-cells, that the surface of the silicon get covered spontaneously with the electrolyte components and products from the degradation of both $LiPF_6$ salt and organic solvents. XPS being more surface sensitive, the detection of LiF by this method, suggests a concentration of the inorganic salt at the electrode surface of the SEI. Once this spontaneous reaction is done, the silicon/electrolyte interface appears to be quite stable. This is further confirmed by the XPS detection of the native Si oxide layer, which is still very thin after aging. Signs of the degradation of the electrolyte appear for 1 month

DOI: 10.1021/acs.chemmater.5b04461
Chem. Mater. 2016, 28, 2557−2572

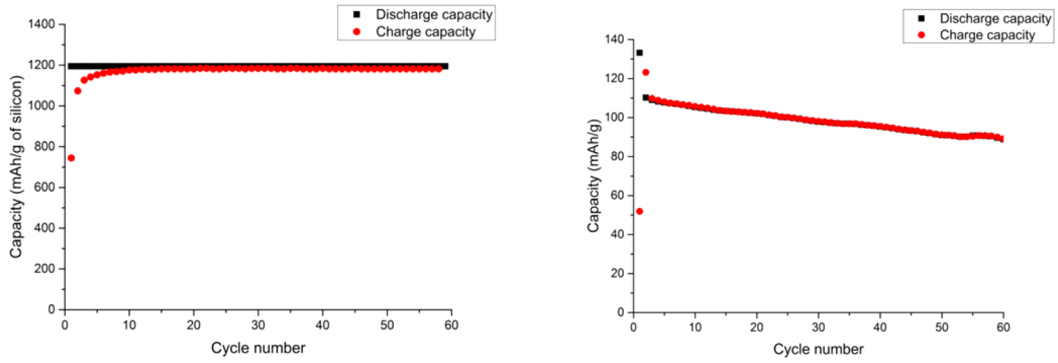

Figure 18. Specific capacity vs cycle number for silicon (left) and NMC (right) "post-mortem" electrodes cycled in half-cell configuration vs lithium metal.

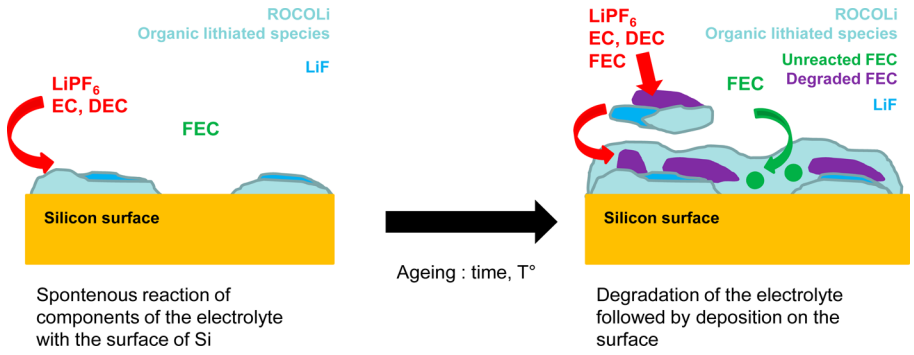

Figure 19. Scheme describing the spontaneous reaction of the electrolyte components with the silicon particle surface and, in a second step, the degradation of the electrolyte with time and/or temperature, including the partial degradation of the FEC additive followed by the deposition of the decomposition products on the surface of the material.

at 25 °C and for 1 day at 55 °C confirming that rapid degradation of the electrolyte can be expected if the functioning temperature of the cell reaches 55 °C. In both cases, a drastic increase of the amount of lithiated species and fluorinated species is observed, confirming that results obtained previously for half-cells stay valid in the case of full Li-ion cells. Products coming from the degradation of the FEC additive are also detected.

After the aging process, the ^{7}Li and ^{19}F NMR spectra are quite different from the ^{7}Li and ^{19}F NMR spectra obtained after 100 cycles. As a matter of fact, the broad resonances at −1.6 ppm in ^{7}Li NMR spectra, indicating the strong degradation process of the electrolyte upon aging, is never observed during the cycling. In a similar way, unreacted FEC as well as FEC degradation products are not observed after an extended cycling at room temperature. These results indicate that the chemical nature of some of the surface species is quite different upon aging from that obtained upon cycling. These results tend also to confirm that a proper efficient SEI is not formed by a simple exposure of the silicon surface to the electrolyte and suggest that the degradation of the electrolyte is more a matter of time (calendar aging) than a matter of electrochemical cycling. Such behavior, at least for full-cell configuration, has been pointed out in the case of $LiFePO_4$/$Li_4Ti_5O_{12}$ system.[47] SXI images (X-ray beam induced secondary electron images) achieved on an aged sample shows heterogeneities at the surface, indicating the nonuniform deposition of degradation products at the surface of the silicon. The whole process is summarized in the following scheme (Figure 19).

Cycling Study. ^{7}Li, ^{19}F MAS NMR, XPS, TOF-SIMS and STEM-EELS characterizations have also provided an in-depth characterization of the SEI forming across the entire electrode, on the surface of silicon particles as well as its evolution upon cycling in a full Li-ion cell configuration with $LiNi_{1/3}Mn_{1/3}Co_{1/3}O_2$ as the positive electrode. Such comprehensive characterization allows for a better understanding of the failure mechanism of Si-based composite electrodes for lithium batteries cycled in full-cell configuration.

In agreement with results obtained in previous studies dealing with half-cells, the formation of the SEI is detected by NMR and XPS during the first lithiation process and is characterized by the presence of LiF and $LiPF_6$ probably trapped in the porosity of the SEI as well as organic species (carbonates, alkyl carbonates) coming from the degradation of EC and DEC solvents. From the very early stages of the electrochemical cycling, the SEI does not appear as a homogeneous layer that would cover all the silicon particles involved in the electrochemical reaction but rather as very heterogeneous deposits comprised of thick patches of LiF and carbonates. Such species are also detected on unreacted silicon particles. Concerning the surface of silicon particles, at the end of the lithiation process, contributions of Li_xSi, Si°, and Li_xSiO_y are detected. Li silicates are known to form after the first cycle and to participate to the irreversibility of the first cycle. It indicates the contribution of the surface of silicon particles in the reaction of SEI formation during cycling, contrary to the case of a simple exposure of silicon to electrolyte. The nature of the chemical species (deduced from XPS and NMR) as well as the heterogeneous nature of the SEI (observed at different

DOI: 10.1021/acs.chemmater.5b04461
Chem. Mater. 2016, 28, 2557−2572

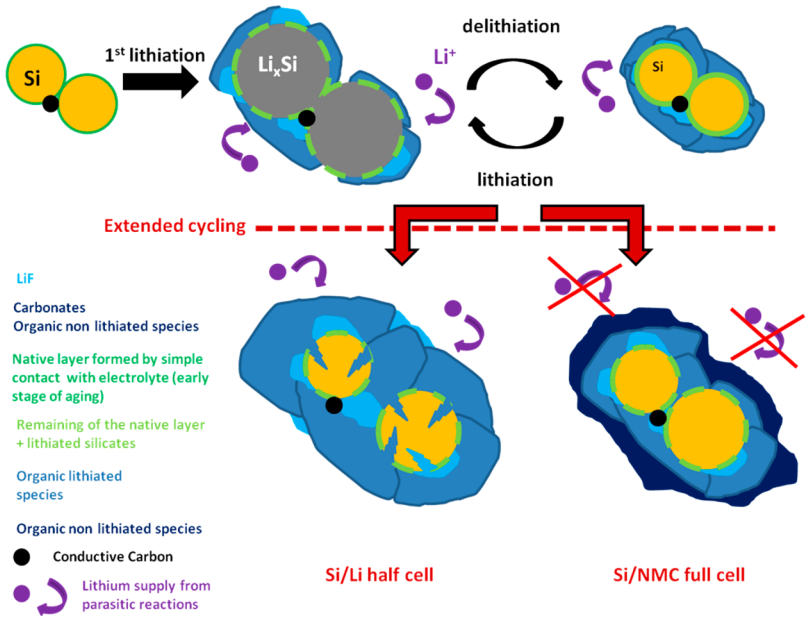

Figure 20. Scheme describing the formation and evolution of the SEI on the surface of silicon particles along the first cycles, occurring similarly for Si/Li half-cell and full Li-ion cell. After an extended cycling, the evolution of the SEI then differs and leads to different final postmortem states.

scales using STEM-EELS and TOF-SIMS) appear quite similar for both half-cells (from previous studies described in the literature) and full Li-ion cells and cannot explain alone such different cycling behaviors.

Qualitative evolutions of the SEI for both half-cell and full Li-ion cells display also some similarities: (i) The development of the inorganic part of the SEI mostly occurs during the early stage of cycling since the contribution of LiF, as seen by NMR and XPS, does not increase over the course of the electrochemical cycling. Conversely, the contribution of organic species such as carbonates continuously increases indicating an incessant degradation of the organic solvents of the electrolyte. (ii) The evolution of the SEI on silicon particles is not only induced by the number of electrochemical cycles but is also sensitive to potential variations between oxidized and reduced states of the silicon electrode and exhibits a significant covering of inorganic species (LiF, Li_xPF_y, and $Li_xPO_yF_z$) by organic species at the end of a delithiation/oxidation process. This indicates (i) a dynamic behavior of the organic part of the interphase and (ii) the formation of some of the organic species during the delithiation step. Nevertheless, in the case of the full Li-ion cells studied here, this variation stabilizes after 10 cycles. Concerning the surface of silicon particles after an extended cycling, results show that (1) Li_xSiO_y is formed in high quantities and (2) Si° signal progressively disappears as both SEI is becoming thicker and less and less Si is available for cycling.

The main and very important difference between SEI evolutions, as it has been described for of half-cell in previous studies and for full Li-ion cell as studied in the present work, lays in the formation of lithium free organic species in the case of the full Li-ion configuration (Figure 20). Although the organic species produced by the degradation of organic solvents seem to be lithiated during the first part of the cycling, carbonate species found in the outer part of the SEI for an extended cycling are clearly not lithiated when silicon is cycled in full Li-ion cell configuration. This result suggests in particular that all the lithium available for cycling has been consumed in parasitic reactions and is either trapped in an intermediate part of the SEI or in the electrolyte. At this point, without any available lithium left for cycling, the cell cannot function properly anymore. This nevertheless does not prevent the further degradation of the EC and DEC organic solvents, simply because of potential variations or calendar aging. The "stacking" trend leading to a distribution of the different species found in the SEI can be directly observed by STEM-EELS, indicating the presence of the thick patches of LiF partially coated by a more covering thin layer of organic products including carbonates. The SEI formation and evolution are summarized in the scheme presented in Figure 20, where differences between half cell (lithiated species present in the whole SEI, cracks and particles disconnection showing the degradation of the electrode) and full cell (non lithiated species at the extreme surface of the SEI, non decrepitated and non disconnected Si particles) appear only for an extended cycling.

In addition, the results obtained indicate that the chemical nature of some of the surface species is quite different whether in aging or in cycling mode. Moreover, species involving clearly a reaction of the silicon surface, such as Li_xSiO_y, are detected only when the battery has cycled and not in the case of a simple exposure to the electrolyte. It tends also to confirm that a proper efficient SEI is not formed by a simple exposure of the silicon surface to the electrolyte and suggests that the progressive degradation of the electrolyte upon electrochemical cycling is a completely different process compared to the calendar aging.

■ CONCLUSIONS

The failure mechanism of silicon-based electrodes has been studied using a combination of ^{7}Li, ^{19}F MAS NMR, XPS, TOF-SIMS and STEM-EELS. This multiprobe approach provides an in-depth characterization of the SEI formation on the surface of silicon and its evolution upon aging and cycling with $LiNi_{1/3}Mn_{1/3}Co_{1/3}O_2$ as the positive electrode in a full Li-ion cell configuration for the first time. STEM-EELS and TOF-SIMS results emphasize the fact that the SEI does not

DOI: 10.1021/acs.chemmater.5b04461
Chem. Mater. 2016, 28, 2557−2572

appear as a continuous and homogeneous layer neither on the electrode scale nor at the nanoparticle scale. Overall, processes of electrolyte degradation occur in full-cell configuration in a similar way compared to Si/Li half-cell, leading to a heterogeneous SEI comprised of LiF and trapped $LiPF_6$ in an organic matrix stemming from the degradation of the electrolyte organic solvents. Such processes cannot explain alone the differences observed in the electrochemical cyclability of half-cells and full Li-ion cells, respectively. Nevertheless, the evolution of the SEI on the silicon surface, for a full-cell configuration, is thus very similar to that in the case of half cells, clearly demonstrating the little influence of the positive electrode on the SEI evolution.

However, the combination of bulk-sensitive MAS NMR and surface sensitive XPS permitted to point out a small but very important difference in the SEI evolution in the case of full Li-ion cell as studied in the present work, compared to the case of half-cell as described in the literature. It lays in the formation of non lithiated organic species at the extreme surface of the SEI in the case of the full Li-ion configuration. Although the organic species produced by the degradation of organic solvents seem to be lithiated during the first part of the cycling, carbonate species found in the outer part of the SEI for an extended cycling are clearly not lithiated when silicon is cycled in full Li-ion cell configuration. This result suggests in particular that all the lithium available for cycling has been consumed in parasitic reactions and is either trapped in an intermediate part of the SEI or in the electrolyte. At this point, after only few cycles and without any available lithium left for cycling, the Li-ion cell cannot function properly anymore. This nevertheless does not prevent the further degradation of the EC and DEC organic solvents, simply because of potential variations or calendar aging.

After an extended cycling in a full Li-ion cell configuration, the NMC and silicon active materials were not degraded or altered and the electronic and ionic percolating networks are still effective indicating that the porosity of the electrodes, in particular the silicon one, are thus not blocked by a thick SEI, contrary to the case of silicon electrodes cycled in the same conditions in half-cell configuration. The failure mechanism of Si/NMC Li-ion cell can then be described solely by large cyclable lithium consumption resulting from parasitic reactions at the negative electrode. The slippage of the positive electrode with respect to the negative one occurs rapidly and progressively. Neither electrodes nor electrode materials are degraded in the process. This process is clearly in agreement with the presence of only non lithiated degradation product in the external part of the SEI. This last result can be pointed out as very important as since it can be considered as a good indicator of which failure mechanism in lithium batteries is occurring first: degradation of the active materials, clogging of the electrode porosity by thick SEI deposits, or shortage of cyclable lithium because of parasitic reactions.

■ ASSOCIATED CONTENT

Supporting Information

The Supporting Information is available free of charge on the ACS Publications website at DOI: 10.1021/acs.chemmater.5b04461.

Electrochemical cycling of silicon and NMC in half-cell configuration, pristine silicon powder characterization, post mortem ^{7}Li MAS NMR on silicon electrodes after 100 cycles in complete Si/NMC Li-ion cell configuration (PDF)

■ AUTHOR INFORMATION

Corresponding Author

*E-mail: Nicolas.dupre@cnrs-imn.fr.

Notes

The authors declare no competing financial interest.

■ ACKNOWLEDGMENTS

This research was funded by the European Research Council (ERC), EU FP7 Energy.2013.7.3.3 program on Understanding interfaces in rechargeable batteries and supercapacitors through in situ methods, Grant Award 608491 on project "Battery and Supercapacitors Characterization and Testing (BACCARA)".

■ REFERENCES

(1) Beaulieu, L. Y.; Eberman, K. W.; Turner, R. L.; Krause, L. J.; Dahn, J. R. Colossal reversible volume changes in lithium alloys. *Electrochem. Solid-State Lett.* **2001**, *4* (9), A137−A140.

(2) Nguyen, B.; Gaubicher, J.; Lestriez, B. Analogy between electrochemical behaviour of thick silicon granular electrodes for lithium batteries and fine soils micromechanics. *Electrochim. Acta* **2014**, *120* (20), 319−326.

(3) Xu, K. Electrolytes and Interphases in Li-ion Batteries and Beyond. *Chem. Rev.* **2014**, *114*, 11503−11618.

(4) Nguyen, C. C.; Song, S. W. Interfacial structural stabilization on amorphous silicon anode for improved cycling performance in lithium-ion batteries. *Electrochim. Acta* **2010**, *55*, 3026−3033.

(5) Baggetto, L.; Niessen, R.; Notten, P. On the activation and charge transfer kinetics of evaporated silicon electrode/electrolyte interfaces. *Electrochim. Acta* **2009**, *54*, 5937−5941.

(6) Winter, M. The Solid Electrolyte Interphase - The Most Important and the Least Understood Solid Electrolyte in Rechargeable Li Batteries. *Z. Phys. Chem.* **2009**, *223* (10−11), 1395−1406.

(7) Oumellal, Y.; Delpuech, N.; Mazouzi, D.; Dupre, N.; Gaubicher, J.; Moreau, P.; Soudan, P.; Lestriez, B.; Guyomard, D. The failure mechanism of nano-sized Si-based negative electrodes for lithium ion batteries. *J. Mater. Chem.* **2011**, *21* (17), 6201−6208.

(8) Mazouzi, D.; Delpuech, N.; Oumellal, Y.; Gauthier, M.; Cerbelaud, M.; Gaubicher, J.; Dupré, N.; Moreau, P.; Guyomard, D.; Roué, L.; Lestriez, B. New insights into the silicon-based electrode's irreversibility along cycle life through simple gravimetric method. *J. Power Sources* **2012**, *220* (0), 180−184.

(9) Liu, W.; Yang, M.; Wu, H.; Chiao, S. M.; Wu, N. Enhanced Cycle Life of Si Anode for Li-Ion Batteries by Using Modified Elastomeric Binder. *Electrochem. Solid-State Lett.* **2005**, *8* (2), A100−A103.

(10) Ryu, J. H.; Kim, J. W.; Sung, Y.; Oh, S. M. Failure Modes of Silicon Powder Negative Electrode in Lithium Secondary Batteries. *Electrochem. Solid-State Lett.* **2004**, *7* (10), A306−A309.

(11) Park, S.; Kim, T.; Oh, S. M. Electrochemical Dilatometry Study on Si-Embedded Carbon Nanotube Powder Electrodes. *Electrochem. Solid-State Lett.* **2007**, *10* (6), A142−A145.

(12) Reyter, D.; Rousselot, S.; Mazouzi, D.; Gauthier, M.; Moreau, P.; Lestriez, B.; Guyomard, D.; Roué, L. An electrochemically roughened Cu current collector for Si-based electrode in Li-ion batteries. *J. Power Sources* **2013**, *239* (0), 308−314.

(13) Lee, S. W.; McDowell, M. T.; Choi, J. W.; Cui, Y. Anomalous Shape Changes of Silicon Nanopillars by Electrochemical Lithiation. *Nano Lett.* **2011**, *11*, 3034−3039.

(14) Beattie, S. D.; Loveridge, M. J.; Lain, M. J.; Ferrari, S.; Polzin, B. J.; Bhagat, R.; Dashwood, R. Understanding Capacity Fade in Silicon Based Electrodes for Lithium-ion Batteries using Three Electrode Cells and Upper Cut-off Voltage Studies. *J. Power Sources* **2016**, *302*, 426−430.

(15) Obrovac, M. N.; Krause, L. J. Reversible cycling of crystalline silicon powder. *J. Electrochem. Soc.* **2007**, *154*, A103−A108.

(16) Mazouzi, D.; Lestriez, B.; Roué, L.; Guyomard, D. Silicon Composite Electrode with High Capacity and Long Cycle Life. *Electrochem. Solid-State Lett.* **2009**, *12* (11), A215−A218.

DOI: 10.1021/acs.chemmater.5b04461
Chem. Mater. 2016, 28, 2557−2572

(17) Kasavajjula, U.; Wang, C.; Appleby, A. J. Nano- and bulk-silicon-based insertion anodes for lithium-ion secondary cells. *J. Power Sources* **2007**, *163*, 1003−1039.
(18) Zhang, W-J. A review of the electrochemical performance of alloy anodes for lithium-ion batteries. *J. Power Sources* **2011**, *196*, 13−24.
(19) Massiot, D.; Fayon, F.; Capron, M.; King, I.; Le Calve, S.; Alonso, B.; Durand, J. O.; Bujoli, B.; Gan, Z.; Hoatson, G. *Modelling one and two-dimensional solid-state NMR spectra*. *Magn. Reson. Chem.* **2002**, *40*, 70−76.
(20) Lucas, G.; Burdet, P.; Cantoni, M.; Hébert, C. Multivariate statistical analysis as a tool for the segmentation of 3D spectral data. *Micron* **2013**, *52*−*53*, 49−56.
(21) Chan, C. K.; Ruffo, R.; Hong, S. S.; Cui, Y. Surface chemistry and morphology of the solid electrolyte interphase on silicon nanowire lithium-ion battery anodes. *J. Power Sources* **2009**, *189*, 1132−1140.
(22) Philippe, B.; Dedryvère, R.; Allouche, J.; Lindgren, F.; Gorgoi, M.; Rensmo, H.; Gonbeau, D.; Edström, K. Nanosilicon Electrodes for Lithium-Ion Batteries: Interfacial Mechanisms Studied by Hard and Soft X-ray Photoelectron Spectroscopy. *Chem. Mater.* **2012**, *24*, 1107−1115.
(23) Etacheri, V.; Haik, O.; Goffer, Y.; Roberts, G. A.; Stefan, I. C.; Fasching, R.; Aurbach, D. Effect of Fluoroethylene Carbonate (FEC) on the Performance and Surface Chemistry of Si-Nanowire Li-Ion Battery Anodes. *Langmuir* **2012**, *28*, 965−976.
(24) Profatilova, I. A.; Stock, C.; Schmitz, A.; Passerini, S.; Winter, M. Enhanced thermal stability of a lithiated nano-silicon electrode by fluoroethylene carbonate and vinylene carbonate. *J. Power Sources* **2013**, *222*, 140−149.
(25) Markevich, E.; Fridman, K.; Sharabi, R.; Elazari, R.; Salitra, G.; Gottlieb, H. E.; Gershinsky, G.; Garsuch, A.; Semrau, G.; Schmidt, M. A.; Aurbach, D. Amorphous Columnar Silicon Anodes for Advanced High Voltage Lithium Ion Full Cells: Dominant Factors Governing Cycling Performance. *J. Electrochem. Soc.* **2013**, *160* (10), A1824−A1833.
(26) Delpuech, N.; Dupré, N.; Mazouzi, D.; Gaubicher, J.; Moreau, P.; Bridel, J. S.; Guyomard, D.; Lestriez, B. Correlation between irreversible capacity and electrolyte solvents degradation probed by NMR in Si-based negative electrode of Li-ion cell. *Electrochem. Commun.* **2013**, *33*, 72−75.
(27) Okamoto, Y. Decomposition Mechanism of Ethylene Carbonate and Fluoroethylene Carbonate through Hydrogen Abstraction under High Voltage Environment: An Ab-Initio Study. *J. Electrochem. Soc.* **2014**, *161* (10), A1527−A1533.
(28) Lux, S. F.; Lucas, I. T.; Pollak, E.; Passerini, S.; Winter, M.; Kostecki, R. The mechanism of HF formation in $LiPF_6$ based organic carbonate electrolytes. *Electrochem. Commun.* **2012**, *14* (1), 47−50.
(29) Lee, Y. M.; Lee, J. Y.; Shim, H. T.; Lee, J. K.; Park, J. K. SEI Layer Formation on Amorphous Si Thin Electrode during Precycling. *J. Electrochem. Soc.* **2007**, *154*, A515−A519.
(30) Philippe, B.; Dedryvère, R.; Gorgoi, M.; Rensmo, H.; Gonbeau, D.; Edström, K. Role of the $LiPF_6$ Salt for the Long-Term Stability of Silicon Electrodes in Li-Ion Batteries - A Photoelectron Spectroscopy Study. *Chem. Mater.* **2013**, *25*, 394−404.
(31) Arreaga-Salas, D. E.; Sra, A. K.; Roodenko, K.; Chabal, Y. J.; Hinkle, C. L. Progression of Solid Electrolyte Interphase Formation on Hydrogenated Amorphous Silicon Anodes for Lithium-Ion Batteries. *J. Phys. Chem. C* **2012**, *116*, 9072−9077.
(32) Key, B.; Bhattacharyya, R.; Morcrette, M.; Seznec, V.; Tarascon, J. M.; Grey, C. P. Real-Time NMR Investigations of Structural Changes in Silicon Electrodes for Lithium-Ion Batteries. *J. Am. Chem. Soc.* **2009**, *131*, 9239−9249.
(33) Gauthier, M.; Mazouzi, D.; Reyter, D.; Lestriez, B.; Moreau, P.; Guyomard, D.; Roué, L. A low-cost and high performance ball-milled Si-based negative electrode for high-energy Li-ion batteries. *Energy Environ. Sci.* **2013**, *6* (7), 2145−2155.
(34) Leveau, L. Etude de nanofils de silicium comme matériau d'électrode négative de batterie lithium-ion. *Doctoral thesis*, l'Ecole Polytechnique, Universite Paris−Saclay, Palaiseau, France, 2015
(35) Radvanyi, E.; De Vito, E; Porcher, W.; Jouanneau Si Larbi, S. An XPS/AES comparative study of the surface behaviour of nano-silicon anodes for Li-ion batteries. *J. Anal. At. Spectrom.* **2014**, *29*, 1120−1131.
(36) Radvanyi; Porcher, W.; De Vito, E.; Montani, A.; Franger, S.; Jouanneau Si Larbi, S. Failure mechanisms of nano-silicon anodes upon cycling: an electrode porosity evolution model. *Phys. Chem. Chem. Phys.* **2014**, *16*, 17142.
(37) Santhanagopalan, D.; Qian, D.; McGilvray, T.; Wang, Z.; Wang, F.; Camino, F.; Graetz, J.; Dudney, N.; Meng, Y. S. Interface Limited Lithium Transport in Solid-State Batteries. *J. Phys. Chem. Lett.* **2014**, *5* (2), 298−303.
(38) Eshkenazi, V.; Peled, E.; Burstein, L.; Golodnitsky, D. XPS analysis of the SEI formed on carbonaceous materials. *Solid State Ionics* **2004**, *170*, 83−91.
(39) Shkrob, I. A.; Zhu, Y.; Marin, T. W.; Abraham, D. Reduction of Carbonate Electrolytes and the Formation of Solid-Electrolyte Interface (SEI) in Lithium-Ion Batteries. 1. Spectroscopic Observations of Radical Intermediates Generated in One-Electron Reduction of Carbonates. *J. Phys. Chem. C* **2013**, *117*, 19255.
(40) Imhof, R.; Novak, P. In Situ Investigation of the Electrochemical Reduction of Carbonate Electrolyte Solutions at Graphite Electrodes. *J. Electrochem. Soc.* **1998**, *145* (4), 1081−1087.
(41) Gourdin, G.; Collins, J.; Zheng, D.; Foster, M.; Qu, D. Spectroscopic Compositional Analysis of Electrolyte during Initial SEI Layer Formation, I. *J. Phys. Chem. C* **2014**, *118*, 17383−17394.
(42) Plakhotnyk, A. V.; Ernst, L.; Schmutzler, R. Hydrolysis in the system $LiPF_6$-propylene carbonate-dimethyl carbonate-H2O. *J. Fluorine Chem.* **2005**, *126*, 27−31.
(43) Edstrom, K.; Herstedt, M.; Abraham, D. P. A new look at the solid electrolyte interphase on graphite anodes in Li-ion batteries. *J. Power Sources* **2006**, *153*, 380.
(44) Cuisinier, M.; Martin, J. F.; Moreau, P.; Epicier, T.; Kanno, R.; Guyomard, D.; Dupre, N. Quantitative MAS NMR characterization of the $LiMn_{1/2}Ni_{1/2}O_2$ electrode/electrolyte interphase. *Solid State Nucl. Magn. Reson.* **2012**, *42*, 51−61.
(45) Cuisinier, M.; Dupre, N.; Martin, J. F.; Kanno, R.; Guyomard, D. Evolution of the $LiFePO_4$ positive electrode interface along cycling monitored by MAS NMR. *J. Power Sources* **2013**, *224*, 50−58.
(46) Marino, C.; Darwiche, A.; Dupré, N.; Wilhelm, H. A.; Lestriez, B.; Martinez, H.; Dedryvère, R.; Zhang, W.; Ghamouss, F.; Lemordant, D.; Monconduit, L. Study of the Electrode/Electrolyte Interface on Cycling of a Conversion Type Electrode Material in Li Batteries. *J. Phys. Chem. C* **2013**, *117* (38), 19302−19313.
(47) Castaing, R.; Reynier, Y.; Dupre, N.; Schleich, D.; Jouanneau Si Larbi, S.; Guyomard, D.; Moreau, P. Degradation diagnosis of aged $Li_4Ti_5O_{12}$/$LiFePO_4$ batteries. *J. Power Sources* **2014**, *267*, 744−752.

DOI: 10.1021/acs.chemmater.5b04461
Chem. Mater. 2016, 28, 2557−2572